Contemporary Approach to Power of Electrostatic Precipitators

Željko V. Despotović

Mihajlo Pupin Institute, University of Belgrade
Department of Robotics
Volgina 15, Belgrade, Serbia
e-mail: zeljko.despotovic@pupin.rs

Slobodan N.Vukosavić, Mladen Terzić

School of Electrical Engineering, University of Belgrade
Chair of Power Converters and Drives
Bulevar Kralja Aleksandra 73, Belgrade, Serbia
e-mail: boban@etf.rs

Abstract—**The supplying of electrostatic precipitators (ESP) significantly affect on the efficiency of fine particle separation from smoke gases as a specific unwanted product of electric energy production on thermal power plants (TPP). In this paper is presented of modern solution of high voltage high frequency (HVHF) power supply of ESP. This solution achieves several significant improvements over the conventional 50Hz, SCR system. It is possible to provide more precise control of the ESP parameters such as the output voltages and currents. It is also possible to make a rapid increase or decrease in voltage and to effectuate a very fast response to load changes. Due to this advantages it is possible to suppress the supply quickly in the case of sparking, reducing the spark energy and the quantity of ionized gasses produced by the electric arc. Reduction in the spark energy is up to 10 times compared to conventional thyristors solution. This paper describe the HFHV power unit AR70/1000, multiresonant topology, principles of operation, simulations and measurement results obtained during extensive experimental investigations on thermal power plants.**

Key words- Thermal power plants; electrostatic precipitators; SCR; multiresonant topology; power converter; IGBT;

I. INTRODUCTION

The environmental pollution problems have become global over the past decade. Widely discussed, they are the outcome of the world wide increase in energy consumption and industrial growth. In turn, the overall amount of waste gasses has increased, including the emission of fine, 1 – 50 µm particles, particularly harmful and being a well-known health risk. Therefore, both large industrial sites and the TPP require dust cleaning equipment and on-line pollution control. Automated control is required for the equipment to operate on its own, without the need for a continuous operator intervention. Control goals include the need to meet the environmental regulations, keeping at the same time the power losses and the overall energy consumption under control, in order to reach the energy efficiency goals [1].

The state of the art dust cleaning methods include the electrostatic precipitators (ESP), forcing the waste gas to flow between large electrode plates, exposed to pulsating DC voltages of several tens of kV. Exposure to high strength electric field charges dust particles and they migrate towards the collecting plate, which is the positive one, and in most cases grounded. The other, negative electrode is attached to the negative supply rail of the controllable DC voltage source. The electrode surface is barbed and equipped with appropriate protruding spikes, responsible for an enhanced ionization. The migration of the charged dust particles takes place due to the electric forces exerted by the field [2]. The drift velocity of the particles and their collection efficiency largely depend on the gas speed and the eventual turbulent flow [3]. To enhance the filtering, the ESP comprise several (up to 8) series connected sections, wherein the output gas from the previous section becomes the input to the next. In such cases, the subsequent section may collect the dust particles that were properly ionized within the previous section, but were not collected due to an insufficient particle drift and/or too large speed of the gas stream.

In an attempt to enhance the ionization, drift speed and filtering, the voltage between electrodes can be increased. Though, along with the voltage increase, corona effects do pass into arcing. The electric arc within the filter effectively short circuits the power source and results in large currents and mass ionization. Following the arcing, the filter should be kept off the power source for several tens of milliseconds in order to allow for the ionized gasses to evacuate. Otherwise, at the reconnection without the de-ionization interval, the filter won't be able to withstand the reconnected voltage and will fall into arcing and short circuit again.

Maximum allowable value of air pollution is 50 mg/m^3 and it requires that the efficiency of the ESP better than 99%, which calls for an increase of active surface of the plates, hence increasing the volume and the weight of steel used for the ESP construction.

In previous decades, electrostatic precipitators in thermal power plants were fed by thyristor controlled-single-phase fed devices [2], [4] having a high degree of reliability, but with relatively low collection efficiency, hence requiring large effective surface of the collection plates and a large weight of steel construction in order to achieve the prescribed emission limits. Collection efficiency and energy efficiency of the electrostatic precipitator can be increased by applying high voltage high frequency (HVHF) voltage power supply.

II. The Conventional Power Supply of ESP

The conventional 50 Hz design of ESP power supply had been predominant solution for controlling the particulate emission from large electrostatic precipitators. In Fig. 1, simplified power supply circuit for the 50Hz, SCR driven ESP is given. Resulting voltages and currents are presented in Fig. 2. Essentially, the plates are supplied with rectified 50Hz waveform. Therefore, the voltage pulsates at a pace of 100Hz, passing quickly the crest value and falling down into dale. Hence, the time interval when the instantaneous voltage is close to the breakdown value, leading to a rich ionization and efficient precipitation, is very short. In brief, the ESP filters only at the peaks of the voltage crest, while operating idle in between the two 10ms spaced crests.
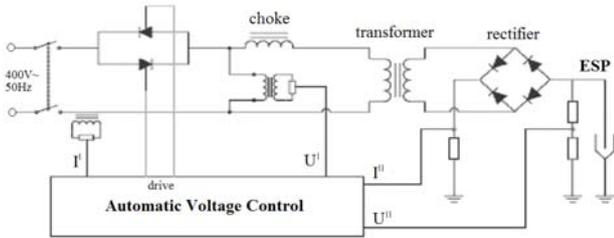

Figure1. Simplified schematic diagram of the 50Hz, SCR power supply unit.
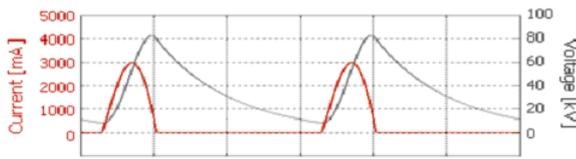

Figure 2. Typical voltage and current waveforms obtained with a 50Hz supplied, SCR driven ESP.

With conventional 50 Hz design, the output DC current is discontinuous, depending on the thyristor firing angle. The input line current is therefore distorted and lagging. As a consequence, the input power factor is very poor, with a high harmonic distortion in the mains supply.

Reactive and apparent power are very large, with $\cos\varphi < 0.65$, whilst power factor $\lambda = P/S < 0.5$. During the intermittent operation of conventional 50Hz system, the ESP pulsations reflect directly to the main 6kV/0.4kV transformer, supplying the whole ESP; as the system does not have any intermediate filters or intermediate DC-link. Low frequency (3-10 Hz) pulsations introduce a flicker, mechanical stress and audible noise.

III. The Modern Power Converter Topology for Supplying of ESP

The efficiency of the precipitation can be increased by providing the retrofit power supply (combination of 50Hz high voltage transformer and current controlled IGBT power converter) which keeps the voltage closer to the breakdown threshold over longer time intervals [5-8].

With high frequency (4 kHz-10 kHz) power supply of the transformer in Fig. 1, the rectified pulses at the output would be spaced 50μs. In such case, due to a finite capacitance of the plates and the associated low pass filtering, the voltage across the plate would be almost ripple-free, without any significant crests and deeps. As a consequence, it would be possible to control the plate voltage more accurately, and keep it next to the breakdown level almost at all times.

In recent years have become very relevant resonant topologies in applications to ESP power [9-13]. Fig. 3, simplified electrical schematics of the high frequency ESP supplies are shown. It comprises: three phase diode rectifier, IGBT full bridge, high frequency high voltage transformer, high voltage, high frequency diode rectifier and L_rC_r resonant link. This link is essentially a resonant circuit. This circuit can be serial resonant circuit (SRC) or parallel resonant circuit (PRC). In Fig.3 (a) is shown series resonant link i.e. SRC, while on Fig.3 (b) is shown parallel resonant link i.e. PRC.
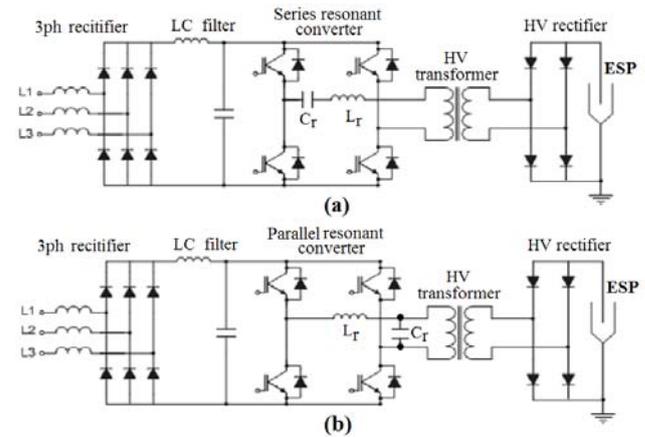

Figure 3. HVHF power converter for ESP power supply having resonant LC circuit, (a) series resonant link, (b) parallel resonant link.

Both of these converters regulate transformer primary voltage by changing the frequency of the driving voltage, such that the impedance of the resonant circuit changes. The input voltage is split between this impedance and the load (high voltage transformer). Since the SRC works as a voltage divider between the input and the load, the DC gain of an SRC is always lower than 1. Under light-load conditions, the impedance of the load is very large compared to the impedance of the resonant circuit; so it becomes difficult to regulate the output, since this requires the frequency to approach infinity as the load approaches zero. Even at nominal loads, wide frequency variation is required to regulate the output when there is a large input-voltage [14].
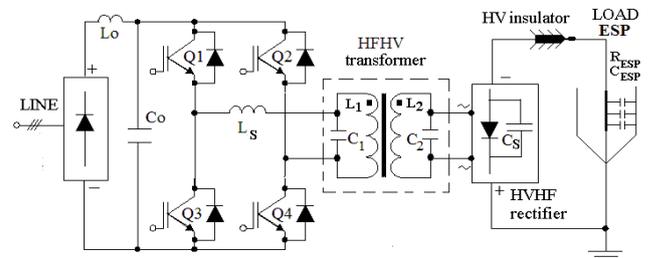

Figure 4. Proposed multiresonant topology of HVHF power supply.
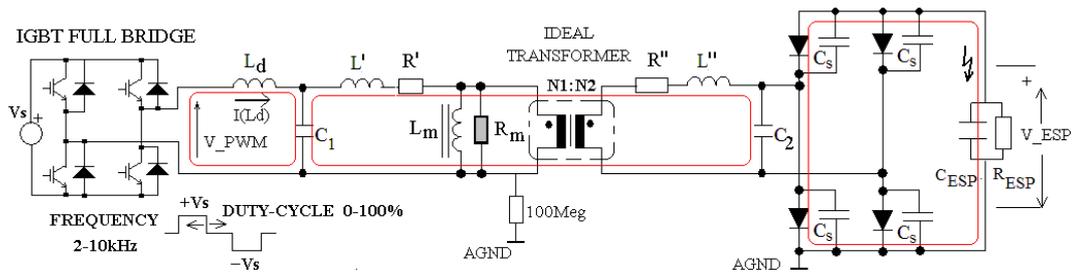
Figure 5. Multi resonant topology of HVHF power supply-simulation scheme.

Due to the distributed configuration of high voltage transformer windings and the existence of distributed capacitance [15-16] in these windings, topology in Fig.3 (b) can be realized with only one element between IGBT- H bridge and primary of transformer, or L inductance. In that case the topology shown in Figure 3(b). In this case the topology in Fig.3 (b) will be presented with multi resonant topology that is shown in Fig.4.

In HVHF topology on Fig.4, are dominant two distributed parasites transformer capacitance C_1 and C_2 on the primary and secondary side, respectively. This capacitances with corresponding inductance $L_1 + L_s$ and L_2 , but as with the capacitance in HVHF rectifier- C_s and ESP plate capacitance- C_{ESP} , form the multi-resonant circuits. Distributed multi-resonant converter topology enables ZCS commutation of IGBT power switches, significantly reduce commutation losses and the insulation stress, hence suppressing the catalytic effects of the electric field high speed changes and preventing chemical reactions leading to accelerated dielectric aging [17]. The output of HVHF rectifier through HV insulator, supply load which consists of parallel connection of high ohmic resistor- R_{ESP} and capacitance C_{ESP} . This load in the first approximation correspond the actual load (the system of collecting and emission electrodes of electrostatic precipitators).

IV.   THE ANALYSIS OF MULTIRESONANT TOPOLOGY AND AUTORI I INSTITUCIJE

The detailed view of the previously described multiresonant topology is given an equivalent scheme which is shown in Fig.5. To analyze this topology is formed multiresonant simulation circuit, which is exciting by high frequency voltage source V_{PWM} ,   with the possibility of changing switching frequency f_{SW} (in range 2-10 kHz) and pulse width i.e. duty-cycle δ (in range 0-100%).

HVHF transformer is presented with equivalent scheme which is consists of several components: resistance and stray reactance of the primary and secondary windings i.e. R' , L' and R'' , L'' , respectively, the magnetization inductance L_m , the equivalent resistance losses in the ferrite core R_m and the parasitic capacitance of the primary and secondary windings

i.e. C_1 and C_2 respectively. In addition to the model used and the ideal transformer fixed transfer ratio $N_1 : N_2$. Input resonance circuit form inductance L_d and the parasitic capacitance C_1 . Significant impact on the work of the entire multiresonant circuit has capacitors that are connected in parallel with the HV diodes. The equivalent capacitance of one branch of a diode rectifier is marked with C_s .

Load parameters R_{ESP} and C_{ESP} on the high voltage side of HVHF supply are taken to correspond to the real case, which has the electrode precipitator system. In the simulation we adopt that the nominal value of the parameters $R_{ESP} = 70 k\Omega$ and C_{ESP} =20nF-40nF.

In the simulation are recorded responses of characteristic values: input current I_{L_d} , voltage of controlled voltage source V_{PWM} , and output load voltage V_{ESP} , for the case of different working regimes of load R_{ESP} : *open-circuit* (OC), *short-circuit* (SC) and rated load of $R_{ESP} = 70 k\Omega$.

It is accepted that the amplitude of voltage source is V_S =540V and the transfer ratio $N_1 : N_2$ of HVHF transformer is equal to 1:100, which is the same as in the real case. The following paper will be presented simulation results for the previously mentioned working regimes.

Fig.6 shows the simulation results for *open-circuit* i.e. when $R_{ESP} = \infty$. In this case, the load is only capacitance C_{ESP} =20nF. In the simulation are obtained waveform of control voltage V_{PWM} , load voltage V_{ESP} and IGBT H-bridge output current I_{L_d} .

At the simulation records on Fig. 6(a) is shown the case when the value of the duty cycle δ is equal to $\delta_1 = 12.5\%$ .Under these conditions, provided the load voltage $V_{ESP1} = 30 kV$, whereas amplitude of output current was $I_{mL_d} = 10$A.

In addition, Fig.6 (b) show the case when the value of the duty cycle is $\delta_2 = 25\%$. In this case is provided the values of the output voltage $V_{ESP2} = 60 kV$, whereas amplitude of input current was 20A.
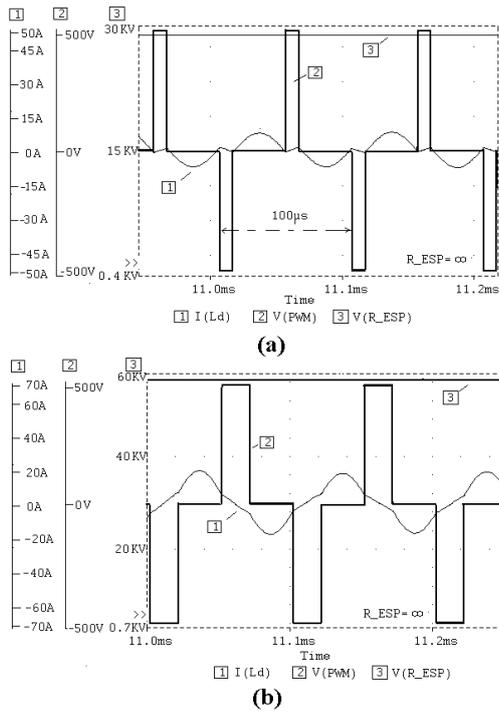
(a)

(b)

Figure 6. Simulation results of multi-resonant power converter for *open-circuit* (OC) to a load at varying of duty cycle δ; (a) δ=12.5%, V_ESP=30kV, (b) δ=25%, V_ESP =60kV.

Fig.7 shows the simulation results for the case of *short-circuit* to a load, i.e. when $R_{ESP} = 0\Omega$. In the simulation are obtained waveform of voltage control voltage V_{PWM} and IGBT H-bridge output current I_{L_d}. The simulation results are shown for the case when the value of the duty cycle is $\delta = \delta_{SC} = 15\%$. Under these conditions, as a result is obtained the value of the input current amplitude of $I_{mL_d} = 45A$.
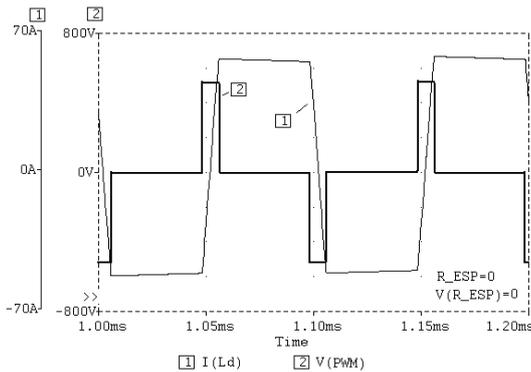

Figure 7. Simulation results of multi-resonant power converter for *short-circuit* (SC) i.e. V_ESP =0V, to a load at duty cycle δ=15%.

Fig.8 shows the simulation results for the case of nominal load regime. Under these conditions they obtained following values: amplitude of the output current was $I_{mL_d} = 150$ A

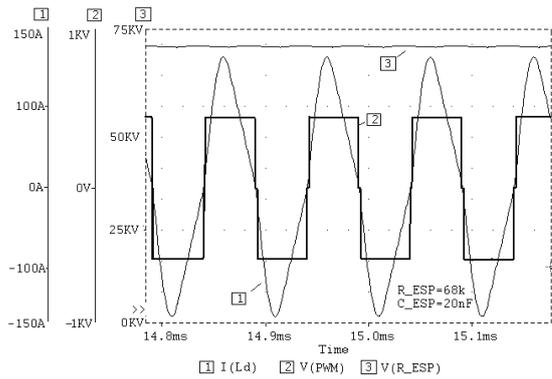(I_{effL_d} = 130A), load current I_{ESP} = 1A and load voltage V_{ESP} = 68kV.

Figure 8. Simulation results of multi-resonant power converter for rated load RESP=68kΩ at duty cycle δ=98%; V_ESP =68kV, I_ESP =1A.

V. THE MULTIRESONANT TOPOLOGY OF ESP POWER-EXPERIMENTAL RSULTS

This section presents the experimental results obtained during the verification and testing multiresonant HVHF power supply AR70/1000. Testing and experimental verification was conducted on TPP "Morava", in the various load regimes: *open-circuit* (no load), *short-circuit*, and the *rated load*.
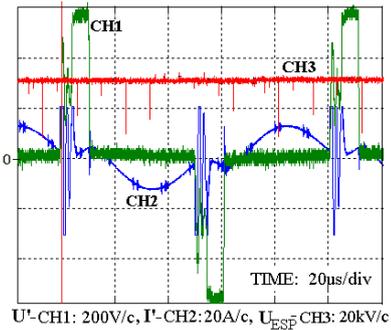

Figure 9. Oscilloscopic records of voltage and current of IGBT converter (CH1 and CH2); 30kV output voltage of HVHF power supply AR70/1000 (CH3).
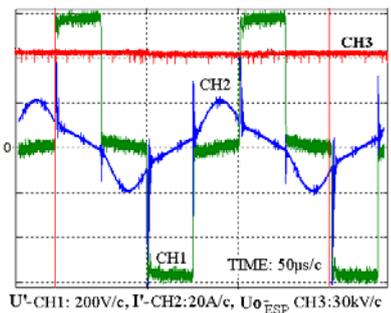

Figure 10. Oscilloscopic records of voltage and current of IGBT converter (CH1 and CH2); 60kV output voltage of HVHF power supply AR70/1000 (CH3).

The conditions under which the experiments were performed to mention: input inductor in the primary circuit of

HF transformer HF, $L_d = 60 \mu H$, the working frequency of IGBT power converter $f_{SW} = 10$ kHz, DC bus voltage $V_s = 540V$.

In Fig.9 are given waveforms of output current and voltage of IGBT converter in no-load regime, where the output high voltage of the AR70 power supply (voltage to the ESP electrodes) was 30kV. Under these conditions the maximum value of the input current was 15A.

In Fig.10 are given the same waveforms in the same mode, where the output voltage of AR70 power supply was 60kV, while the maximum value of the input current was 20A.
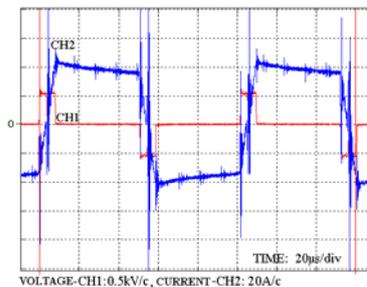

VOLTAGE-CH1:0.5kV/c, CURRENT-CH2: 20A/c

Figure 11. Oscilloscopic records of voltage and current of IGBT converter (CH1 and CH2); Short circuit of HVHF power supply AR70/1000; "duty cycle" δ = 15%.

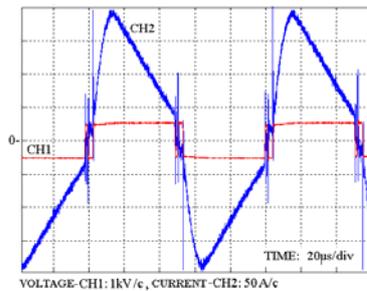VOLTAGE-CH1: 1kV/c , CURRENT-CH2: 50A/c

Figure 12. Oscilloscopic records of voltage and current of IGBT converter (CH1 and CH2); full load 70kV/1000mA of HVHF power supply AR70/1000.

In Fig.11 are shown oscilloscopic records of primary voltage and current of HVHF transformer in *short-circuit* on the output of AR70 power supply. This mode is performed at reduced voltage ("duty cycle" was δ = 15%) to the primary side of the current amplitude was 40A.

In Fig.12 are given oscilloscopic records for full load of HVHF power supply AR70/1000.

In the following are the experimental results obtained by comparing the conventional SCR-50Hz system with the new multiresonant HVHF power supply system.

With conventional SCR-50 Hz system, the breakdown occurs at the crest of rectified sinusoidal voltage half-wave. Thus, amplitude of half-wave should not cross breakdown voltage. The mean voltage is lower (maximum mean value is $2U_{max} / \pi$. Therefore, the average of the squared voltage at the ESP is roughly twice lower than the breakdown voltage squared. On the other hand, the HVHF can control the ESP voltage with a minimum voltage ripple, keeping it close to the breakdown level where needed. Hence, as a rough estimate, the HVHF power offers the high voltage on the electrodes

which has the average square value twice larger than the one encountered with a 50Hz system, show in Fig. 13. High frequency power supply has a negligible ripple, below 1%, and the mean value of voltage can achieve 98.5% of U_{max}.

CH1: ESP voltage (50Hz SCR power)   20kV/c
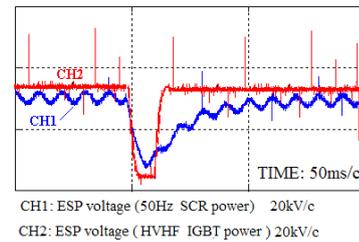CH2: ESP voltage (HVHF IGBT power) 20kV/c

Figure 13. The comparison of ESP voltage waveforms and of ESP reaction to the flashover for SCR- 50Hz and HVHF power.

With the power supply no longer dependent on the mains frequency, the response time of the system will be shortened by an order of magnitude. The HVHF power reacts in hundreds of microseconds, and it quickly minimizes the adverse effects of flashover, such as the short circuit current spikes, massive ionization, and a significant de-ionization time. As a consequence, the ESP can operate much closer to the breakdown voltage, with a very low incidence of flashover, increasing thus the particle filtering. With the HVHF supply reaction time is below 500μs (Fig. 13). Conventional 50Hz supply has the reaction time of 10 ms or more. Result is a significant improvement of precipitator performances in terms of energy saving and improving the collection efficiency.

CH1- POWER NETWORK VOLTAGE   200V/c
CH2- INPUT CURRENT (SCR 50Hz system) 200A/c
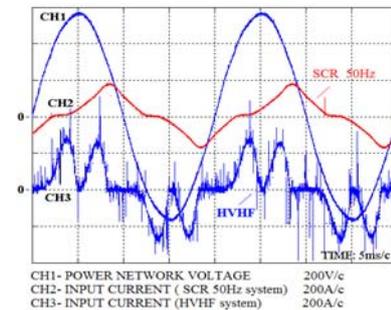CH3- INPUT CURRENT (HVHF system)   200A/c

Figure 14. The comparison of input current of SCR-50Hz and HVHF power converter for ESP supplying.

Fig.14 presents the experimental results of comparing the input current waveform of a conventional SCR and a new HVHF system of power. With conventional SCR-50 Hz design, the output DC current is discontinuous, depending on the thyristor firing angle. The input line current is therefore distorted and lagging. As a consequence, the input power factor is very poor, with a high harmonic distortion in the mains supply. Reactive and apparent power are very large, with $\cos\varphi < 0.65$, whilst power factor $\lambda = P / S < 0.5$. On the other hand, the HVHF supply has three-phase diode rectifier in input stage with $\cos\varphi$ above 0.95 and power factor above 0.75. In addition to obtained experimental results, in Table-I are given the comparison of the power factor and the efficiency with conventional and high frequency power supply.

TABLE I. THE COMPARISON OF CONVENTIONAL AND MODERN ESP POWER

	SCR-50Hz power system	HVHF ESP power system
$cos\varphi$	< 0.65	> 0.95
λ=P/S	< 0.5	> 0.75
η (%)	< 60	> 97

In addition to the previously presented experimental results, the following are the results to relate on particulate monitoring and measurement of output concentration particle at the ESP plant of TPP "Morava". Fig.15 shows the obtained results. The left part of the figure shows the emission difference in case of using the HVHF supply. The transition from HVHF system to 50Hz system was made in the middle (very high particle emission- both ESP power are off).
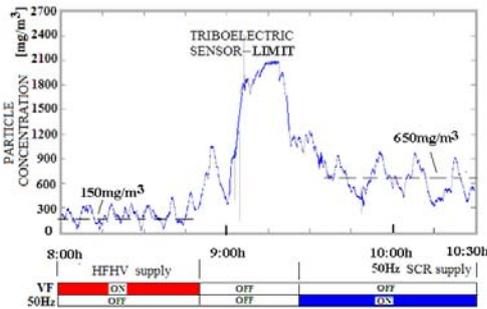

Figure 15. The particulate monitoring and measurement of the output concentration of particle.

The right part of the figure shows the emission change from SCR-50 Hz units. In the observed figure it is noticed that the HVHF supply diminishes the emission from 650 mg/m^3, which is obtained for the supply from 50 Hz T/R units, to only 150 mg/m^3.

VI. CONCLUSIONS

During these four years, a series of tests was performed in order to investigate the impact of HVHF power supplies on the ESP operation. HFHV power supply AR70/1000 is in the exploitation conditions proved very successful. Distributed multiresonant topology in the secondary circuit enables reducing of commutation losses and the insulation stress, hence suppressing the catalytic effects of the electric field high speed changes and preventing chemical reactions leading to accelerated dielectric aging. By measuring the voltage and current waveforms at TPP "Morava", as well as by logging the gas opacity data, it is concluded that the HVHF supply gives the following improvement in relation to conventional SCR-50 Hz supply:

- Spark energy is decreased four to five times,
- Energy includes the amount supplied through the thyristors until they cease to conduct; the HVHF power supply reduces the spark energy down. Namely, the residual spark energy is the one accumulated in the electric field between the electrodes, as the HVHF source itself has a negligible contribution due to a quick turn-off of IGBT power switches,
- In case of occurrence of an arc or spark, the deionization power-down interval is very short, ranging only 2 ms -10 ms, so that the effects of the power interruption on the dust emission becomes very small,
- According to the evaluation, the necessary surface of electrodes is diminished by 30%,
- It is possible to enable quick voltage changes in coordination with the rapping, further enhancing the ESP efficiency.

LITERATURE

[1] N.V.P.R Durga Prasad, T.Lakshminaray, J.R.K Narasimham, T.M.Verman and C.S.R Kirshnam Raju, "Automatic Control and Management of Electrostatic Precipitator", IEEE Trans. on Industry Applications, Vol.35, No.3, May/June 1999, pp.561-567.

[2] K. Parker, Electrical operation of electrostatic precipitators, The Institution of Electrical Engineers, London, 2003.

[3] Laurentiu M. Dumitran, Pierre Atten, Didier Blanchard, and Petru Notingher, " Drift Velocity of Fine Particles Estimated From Fractional Efficiency Measurements in a Laboratory-Scaled Electrostatic Precipitator " IEEE Trans. on Industry Applications, vol. 38, no. 3, pp. 852-857, May/June 2002

[4] P.Boyle, G.Paradiso, P.Thelen, "Performance Improvements From Use of Low Ripple Three- Phases Power Supply for Electrostatic Precipitator", Proceedings of American Power Conference-Vol.61-1, Illinois Institute of Technologys,Feb.1999., Chicago , USA.

[5] Norbert Grass, "150kV/300kW High Voltage Supply with IGBT Inverter for Large Industrial Electrostatic Precipitator", Industry Applications Conference, 2007, 42nd IAS Annual Meeting of the 2007, pp. 808-811.

[6] Norbert Grass, Werner Hartmann, Michael Klöckner, "Application Of Different Types Of High-Voltage Supplies On Industrial Electrostatic Precipitators", IEEE Trans. on Industry Applications, vol. 40, no. 6, pp. 1513-1520, Nov/Dec 2004.

[7] N. Grass, "Fuzzy logic-optimizing IGBT inverter for electrostatic precipitators," IEEE-IAS Annual. Meeting, vol. 4, Phoenix, AZ, Oct. 4–7, 1999, pp. 2457–2462.

[8] S.Vukosavic, Z.Despotovic, N.Popov,"Retrofit Power Supply of Electrostatic Precipitators on Thermal Power Plant-Morava", PROCEEDINGS of the XVI International Symposium of the Power Electronics, N.Sad 26-28.X.2011, Vol.T1-1.9, pp. 1-5.

[9] P. Ranstad, C. Mauritzson, M. Kirsten, and R. Ridgeway,"On experiences of the application of high-frequency power converters for ESP energization," International Conference on Electrostatic Precipitation ICESP 2004.

[10] Sanbao Zheng and Dariusz Czarkowski, "High-Voltage High-Power Resonant Converter For Electrostatic Precipitator", in APEC Conf. Record 2003.vol. 2, pp. 1100-1104.

[11] J. Liu, Sheng, J. Shi, Z. Zhang, X. He, "LCC Resonant Converter Operating under Discontinuous Resonant Current Mode in High Voltage, High Power and High Frequency Applications", in Applied Power Electronics Conference APEC2009, pp. 1482-1486.

[12] R. L. Streigerwald, "A Comparison of Half-Bridge Resonant Converter Topologies" in IEEE Trans. on PE, vol 3, no. 2, April 1988, pp. 174-182

[13] Ž.Despotović, S.Vukosavić, D.Arnautović, I. Stevanović "Visokofrekventno napajanje i njegov uticaj na kvalitet rada ESI", ELEKTROPRIVREDA,Vol.4, pp.132-143, Dec. 2008 (in serbian).

[14] H.Huang, "Designing an LLC Resonant Half-Bridge Power Converter", http://focus.ti.com/asia/download/Topic_3_Huang_28pages.pdf

[15] John C. Fothergill, Philip W. Devine, and Paul W. Lefley, "A Novel Prototype Design for a Transformer for High Voltage, High Frequency, High Power Use", in IEEE Trans. on Power Delivery, vol. 16, no. 1, January 2001. pp. 89-98.

[16] Ž.Despotović, S.Vukosavić, "Razvoj prototipa visokonaponskog visokofrekventnog transformatora za napajanje elektrostatičkih izdvajača", ELEKTROPRIVREDA, Godina:LXIII Vol.2, pp.107-116, Septembar 2010 (in serbian).

[17] H.A.Pohl, Dielectrophoresis. Cambridge: Cambridge University Press, 1978.